Insights into excited-state and isomerization dynamics of bacteriorhodopsin from ultrafast transient UV absorption

S. Schenkl, F. van Mourik, N. Friedman, M. Sheves, R. Schlesinger, S. Haacke, and M. Chergui

PNAS 2006;103;4101-4106; originally published online Mar 6, 2006;
doi:10.1073/pnas.0506303103

Insights into excited-state and isomerization dynamics of bacteriorhodopsin from ultrafast transient UV absorption

S. Schenkl*, F. van Mourik*, N. Friedman†, M. Sheves†, R. Schlesinger‡, S. Haacke*§, and M. Chergui*¶

*Laboratoire de Spectroscopie Ultrarapide, Institut des Sciences et Ingeniérie Chimiques, Faculté des Sciences de Base, Ecole Polytechnique Fédérale de Lausanne, CH-1015 Lausanne-Dorigny, Switzerland; †Departments of Organic Chemistry and Chemical Services, The Weizmann Institute of Sciences, Rehovot 76100, Israel; and ‡Institute for Structural Biology, Forschungszentrum Jülich, 52425 Jülich, Germany

Edited by Robin M. Hochstrasser, University of Pennsylvania, Philadelphia, PA, and approved January 12, 2006 (received for review July 27, 2005)

A visible-pump/UV-probe transient absorption is used to characterize the ultrafast dynamics of bacteriorhodopsin with 80-fs time resolution. We identify three spectral components in the 265- to 310-nm region, related to the *all-trans* retinal, tryptophan (Trp)-86 and the isomerized photoproduct, allowing us to map the dynamics from reactants to products, along with the response of Trp amino acids. The signal of the photoproduct appears with a time delay of ≈250 fs and is characterized by a steep rise (≈150 fs), followed by additional rise and decay components, with time scales characteristic of the J intermediate. The delayed onset and the steep rise point to an impulsive formation of a transition state on the way to isomerization. We argue that this impulsive formation results from a splitting of a wave packet of torsional modes on the potential surface at the branching between the *all-trans* and the cis forms. Parallel to these dynamics, the signal caused by Trp response rises in ≈200 fs, because of the translocation of charge along the conjugate chain, and possible mechanisms are presented, which trigger isomerization.

ultrafast spectroscopy | retinal proteins | translocation of charge | structural dynamics

The different biological functions of retinal proteins (vision, ion pumping, light signaling, etc.) rely on the ultrafast isomerization of the retinal chromophore (1). This process has been intensively investigated by fs pump-probe and fluorescence up-conversion spectroscopy in the visible (VIS) and/or near-IR (2–13), revealing the retinal excited-state dynamics before isomerization and the build-up of the isomerized form. Time-resolved VIS-pump/mid-IR probe experiments on bacteriorhodopsin (bR) established that the isomerization time is ≥400 fs (14). Indeed, the excited-state lifetime of 300–500 fs (12, 15) goes hand-in-hand with the rise times observed for the 13-cis photoproduct (3, 4, 14), whereas a longer time scale of 3–4 ps has been attributed to vibrational relaxation of the photoproduct (14).

The mechanism leading to the isomer is still subject to debate. Using <5-fs pulses, Kobayashi *et al.* (11) were able to monitor changes in the high-frequency vibrational spectrum of the excited state, suggesting that retinal is in a twisted, nonplanar configuration during the initial 200 fs. They also showed that the high-frequency modes were modulated with a period of ≈200 fs, corresponding to the low-frequency torsional modes observed in transient absorption experiments at 800-nm probe wavelength (16). That the system is *all-trans*-like during the first 200 fs is in line with Zhong *et al.* (17), who carried out transient absorption studies on wild-type bR and bR reconstituted with retinal analogs that cannot undergo isomerization and found identical dynamics during the initial 200 fs. In addition, McCamant *et al.* (18) recently showed by fs-stimulated Raman spectroscopy that the high-frequency modes (1,000–1,500 cm^{-1}) decay on a time scale of ≈250 fs. They argued that this observation points to the excited-state population evolving to a new, Raman-silent configuration. They further suggested that the initially active Franck–Condon modes relax to lower-frequency modes that are not directly excited by the pump pulse.

All of these studies point to a dynamical process in the first 200–250 fs, which precedes isomerization and activates the low-frequency torsional modes. In a recent report (19), we presented results of a fs VIS-pump/UV-probe transient absorption study of bR, in which we followed the response of the tryptophan (Trp) residues close to retinal, after excitation of the latter. We found that the Trp response evolves on a time scale of 150–200 fs and showed that it results from the long-hypothesized (20, 21) translocation of charge along excited retinal, which increases the difference dipole moment with respect to the ground state. The translocation of charge therefore appears to temporally coincide with the decay of the high-frequency modes, yet its exact role in the isomerization process is not known. In addition, given that the coherence of the low-frequency torsional modes lasts longer (11, 16) than the isomerization time (14), the question is raised as to a coherent formation of the photoproduct. Indeed, in the case of rhodopsin, impulsive formation of the *all-trans* photoproduct was reported (22), which then undergoes low-frequency coherent oscillations observed over 2 ps.

The use of UV probe wavelengths near 300 nm opens intraretinal observation windows, which provide additional insight into the ultrafast dynamics. Here, we report on transient absorption measurements, with specific spectroscopic fingerprints of the *all-trans* retinal, the Trp, and the photoproduct, and we identify the formation of a transition state by an impulsive mechanism, caused by arrival of a wave packet of torsional modes along the isomerization coordinate. We believe that this particular behavior was hidden in the traditionally investigated red part of the spectrum (600–800 nm) (3, 5, 9, 23), because of overlapping absorption and stimulated emission contributions of the *all-trans* and cis photoproduct. We also present mechanisms by which the translocation of charge along retinal triggers the isomerization, once the system is in the transition state.

Results

Figs. 1 and 2 show a representative selection of the transient absorption changes between 265 and 306 nm of WT bR upon excitation at 560 nm. Similar transients were obtained for the W182 mutant, to which we come back later.

Conflict of interest statement: No conflicts declared.

This paper was submitted directly (Track II) to the PNAS office.

Abbreviations: VIS, visible; bR, bacteriorhodopsin.

§Present address: Groupe d'Optique Nonlinéaire et d'Optoélectronique, Institut de Physique et Chimie des Matériaux de Strasbourg, 23 Rue du Loess, F-67034 Strasbourg Cédex, France.

¶To whom correspondence should be addressed. E-mail: majed.chergui@epfl.ch.

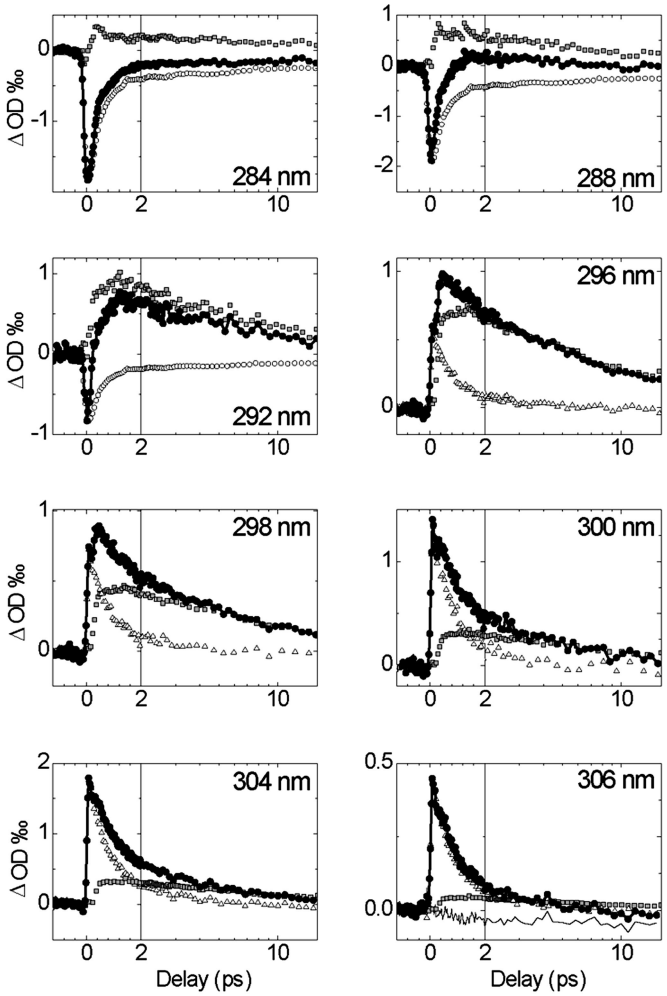

Fig. 1. Femtosecond VIS-pump/UV-probe transients of bR obtained after excitation of retinal at 560 nm with 25-fs pulses. Experimental data points (●) show bleach and excited-state absorption features when going from short to long wavelengths. The contributions of the three pure transients are displayed: F_1 (○), F_2 (squares), and F_3 (triangles). The OD changes are ≈30 times smaller than in the VIS part of the bR spectrum, when excited with similar pulse energies.

The bleach transients, already discussed in ref. 19, are identical for probe wavelengths from 265 to 280 nm (Fig. 2). Between 280 and 294 nm, a positive contribution adds up to the bleach, gradually building up, to become overwhelming. Above 296 nm, the signal is entirely positive, with a first component, which is steeply rising at early times, followed by a second component showing an additional rise and a multiexponential decay. These features are best seen in Fig. 3 *Inset*, where we reproduce the early times of the 296-nm transient. The relative contributions of the two components change as the probe wavelength is tuned to the red, with the early time component ultimately dominating the signal for the red-most probe wavelengths. The data provide an intrinsic clock of the dynamics as the rise of the bleach signals at ≤284 nm is clearly longer than that of the positive signals (best seen on the transients at ≥300 nm), the latter coinciding with the cross correlation (Fig. 6, which is published as supporting information on the PNAS web site, shows a direct comparison between the 280- and 300-nm transients, where the different rise times appear clearly). The multicomponent character of the transients observed at λ ≥296 nm is seen in Fig. 3, where we show the best fit, obtained by using a sum of four exponentials. The fit

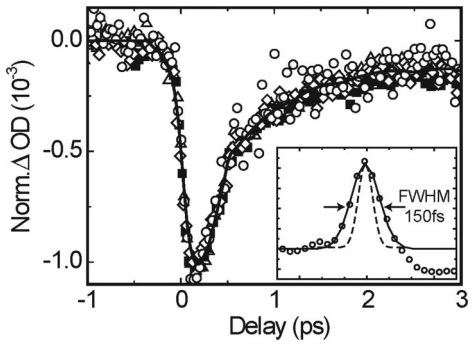

Fig. 2. Normalized VIS-pump/UV-probe transients at probe wavelengths of 265 nm (○), 270 nm (triangles), 275 nm (■), and 280 nm (diamonds). The perfect overlap of the transients suggests a signature of a single species. (*Inset*) The first derivative of the bleach trace (○) has a full width at half maximum (FWHM) of 150 fs, which is significantly longer than the cross correlation of 80 fs (dashed line).

can evidently not capture the component at early times. Obviously, by increasing the number of rising and decaying exponential components, the residual at early times can be reduced, but at the cost of an unrealistically large number of time constants (≈6), which in addition, bear little relation with those reported for bR (3, 4, 14). Clearly, the assumption of purely exponential kinetics is inadequate to analyze our data. Therefore, we refrain from using standard global fitting algorithms (24–26) or Laplace transform approaches (27, 28), all of which rely on the assumption that the kinetics are exponential. We use our recursive kinetic data decomposition approach, described in detail in *Supporting Text*, which is published as supporting information on the PNAS web site. Briefly, it consists of extracting pure kinetic traces from the data, in an iterative way, until all pure kinetic traces that make up the data are isolated.

The choice of the first component $F_1(t)$ is based on the observation that the shape of the time-resolved signals does not change from 265 to 280 nm (Fig. 2). It is very unlikely that in such a large energy range two different kinetic traces are always contributing with exactly the same amplitude ratio. Therefore, the entire bleach at ≤280 nm can be considered to be a "pure" transient (i.e., associated to one process). The kinetic traces for 282- to 294-nm probe wavelengths (Fig. 1) obviously differ from $F_1(t)$ but show a contribution of the latter and additional components $F_i(t)$. The wavelength-dependent amplitudes $A_1(\lambda)$ are adjusted such that they account for the early negative portion

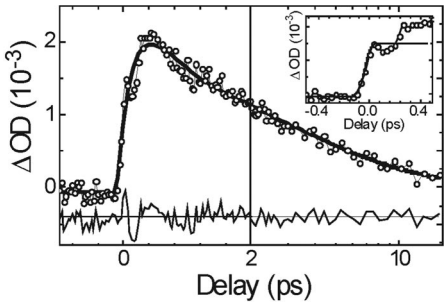

Fig. 3. Kinetic trace at 296 nm (○) together with the best fit (solid line) using sums of exponentials: a 270-fs rise time and three decay components with time constants of 500 fs, 3.0 ps, and 13.7 ps. The residuals of the fit (solid line, bottom) show strong deviations around time 0, demonstrating the inadequacy of the exponential fit. (*Inset*) Early time response and fit (solid line) of the initial part of the signal, showing that it rises within the cross correlation, whereas the second component is delayed leading to the maximum at ≈500 fs.

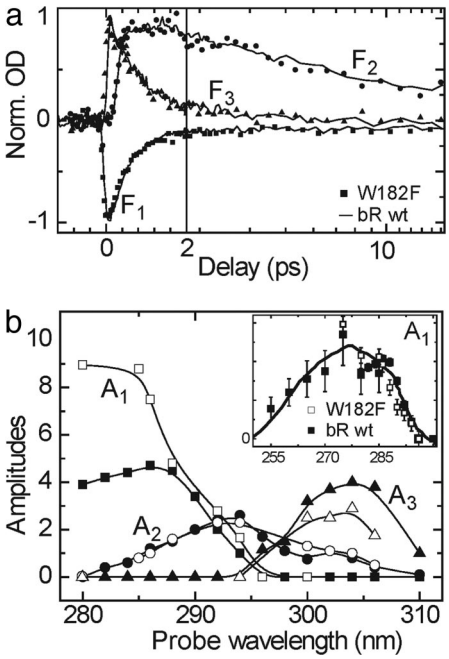

Fig. 4. Kinetic traces and their wavelength dependence, extracted from the data (Fig. 1). (*a*) The three pure transients F_i as obtained from the recursive kinetic data decomposition analysis for WT bR (lines) and the mutant W182F (symbols). (*b*) Their spectral amplitudes A_i as a function of probe wavelength for the Trp bleach (A_1, squares), the isomerized photoproduct absorption (A_2, circles), and the excited-state absorption (A_3, triangles). (*Inset*) Comparison of the A_1 trace with the $S_0 \rightarrow L_a$ component of the Trp absorption (solid line) in propylene glycol (40), blue-shifted by 5 nm to account for the lower polarity of the protein.

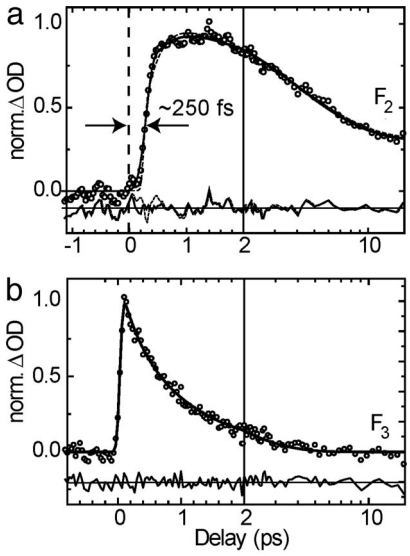

Fig. 5. The F_2 (*a*) and F_3 (*b*) transients and their fits, along with their residuals. Experimental data are ○. In *a*, the solid line represents the fit with a delayed Gaussian (half width at half maximum ≈150 fs) for the steep rise, followed by an exponential rise (≈470 fs) and decay (≈3.8 ps). The dashed line represents the fit with only a rising (≈300 fs) exponential and a decaying (≈3.8 ps) component. In *b*, the fit was done with a biexponential function (with 290-fs and 1.1-ps time constants), while the rise is cross-correlation limited. See text for details.

of these time traces. Subtracting $A_1(\lambda)\,F_1$ from the kinetic traces at 282–294 nm results in residuals with a steeply rising component, followed by a slower rise and a decaying component (squares in Fig. 1). The steep rise does not start at $t = 0$, as confirmed by averaging these residuals, which then form the second transient F_2, shown in Fig. 4*a*. As at the blue-most wavelengths the amplitude of this component is relatively small (Fig. 1), only the F_2 contributions in the kinetic traces from 288 to 294 nm were considered for the average.

As the bleach feature disappears for $\lambda > 294$ nm, it is very plausible to assume that $A_1(\lambda)$ is negligible for increasing wavelengths. The amplitude of F_2, however, is still increasing for larger λ and dominates the signal at 292 and 296 nm. The delayed rise of F_2 is consistent with the peculiar two-step rise behavior of the kinetic traces ≈296 nm (Fig. 3). For probe wavelengths $\lambda > 296$ nm, the kinetic traces exhibit the components mentioned above: a first steeply rising one at $t = 0$, followed by additional, delayed rising and decaying components caused by F_2. The first steep rise obviously suggests the existence of a third positive component, F_3. When subtracting $A_2(\lambda)F_2$ from the time-resolved signals of 300–304 nm [the $A_2(\lambda)$ amplitude is adjusted by assuming that it dominates the signal amplitude at long delay times (8–13 ps)], we obtain the third component, F_3, shown as triangles in Fig. 1. Remarkably enough, the recovered F_3 traces are identical at all probe wavelengths, confirming the consistency of our decomposition. As F_2 and F_3 contribute with comparable strength to the kinetic traces at 296 and 298 nm, their amplitudes have been adjusted by a nonlinear fit algorithm using all three F_is. It turns out that using F_1 does not really improve the fit, and we exclusively used F_2 and F_3 for these wavelengths. The data on the W182 mutant were independently decomposed by the same method, and the resulting transients overlap perfectly those of the WT (Fig. 4*a*), supporting once more the consistency of our decomposition.

One may argue about the small differences between the transient F_2 and the residuals found after subtracting F_1 in the kinetic traces of 284 and 288 nm (Fig. 1). If we carry out the decomposition in the other direction, i.e., subtracting the F_2 transient from the shorter wavelength time traces, the residuals of all decay curves match well with the F_1 transient, which is the dominating contribution at these wavelengths. Therefore, we disregard the small variations in the F_2 fit transient. For 306 nm and further to the red, an additional low-amplitude component, F_4, is needed to reproduce the data (solid line in Fig. 1). This component is probably caused by ground-state bleach in a retinal absorption band at 306 nm and will not be discussed here.

F_3 is the only transient that rises within the cross-correlation time from $t = 0$. The fit of F_3 (Fig. 5*b*) reveals two decay times: $\tau_1 = 290$ fs (amplitude $A_1 = 0.25$) and $\tau_2 = 1.1$ ps ($A_2 = 0.75$), although constants such as $\tau_1 = 600$ fs ($A_1 = 0.7$) and $\tau_2 = 2$ ps ($A_2 = 0.3$) fit just as well the curve. Our weak UV signals do not allow us to specify the decay times with more precision. F_2 exhibits an onset at 250 ± 20-fs delay, followed by a steep rise and an additional slower rise, that precedes a decay. It is best-fitted by using, for the steep rise, a Gaussian with a half width at half maximum of ≈150 fs, and exponentials consisting of a rising component of 470-fs time constant and a decay component of 3.8-ps time constant, until the signal reaches a constant long-time offset (Fig. 5*a*). An alternative fit with a 300-fs rising component and a 3.8-ps decay shows more deviations, especially in the signal rise (dashed lines, Fig. 5*a*). The delayed rise of F_2 is in full agreement with the peculiar structure of the long-wavelength transients mentioned above (Fig. 1, 296–306 nm). In these transients, F_3 is responsible for the fast rise and the "peak" at early times, whereas F_2 generates the characteristic shoulder at later times (400–800 fs). The need for a time delay of ≈250 fs is most clearly seen in the shape of the 296-nm signal transient, where the signal is maximal at 400–500 fs (Fig. 3). The peak in the rising edge dominating at 304 and 306

nm can only be reproduced by a sharply rising F_3. These observations justify *a posteriori* the above assumptions for adjusting the amplitudes used in the sequential subtractions. F_1, the only bleach transient, exhibits a rise time longer than the cross correlation, as already discussed in ref. 19. It rises on a 150- to 200-fs time scale and recovers in a biexponential fashion with time constants of $\tau_1 = 420$ fs, $\tau_2 = 3.5$ ps, typical of retinal, and a constant signal τ_∞ (19).

The wavelength-dependent amplitudes of the transients $F_i(t)$ are shown in Fig. 4*b* for WT bR and the W182F mutant. Just as with the kinetic traces (Fig. 4*a*), similar spectral features appear for both species. As already discussed (19) and shown in Fig. 4 *Inset*, $A_1(\lambda)$ maps the Trp absorption. $A_2(\lambda)$ has a maximum at 294 nm and, probably, a second one at 302 nm. Spectrum $A_3(\lambda)$ has an onset at 296 nm and a maximum ≈305 nm. Interestingly, $A_1(\lambda)$ is nearly twice as intense in the mutant as in WT bR, whereas $A_3(\lambda)$ appears more intense in the latter.

Discussion

Having identified three individual transients, we now examine their time dependence in more detail and their assignment to either of the two chromophores involved in these experiments, namely retinal and Trps. Finally, the ultrafast kinetics is discussed in relation to studies carried out by probing the response of retinal itself.

The Tryptophan Response. We already discussed the reasons to attribute transient F_1 to Trp-86 (19). Briefly, these were: (*i*) The transients are independent of the probe wavelength over >2,000 cm^{-1} (265–280 nm), suggesting that a single species contributes. (*ii*) It cannot originate from retinal, as a retinal bleach transient would follow the instrument response without additional rise time (Fig. 2). (*iii*) The wavelength dependence of the maximum amplitude maps very well the L_a-absorption band of Trp, as seen in Fig. 4*b Inset*. (*iv*) The response is identical in the W182 mutant.

The Trp response mirrors the changes of the permanent dipole moment of retinal after excitation, as was rationalized by modeling the excitonic coupling between retinal and the nearest two Trps (86 and 182) (19). The sudden dipole moment change of retinal in the Franck-Condon region at $t = 0$ (29, 30) is followed by a progressive increase of the difference dipole moment, $\Delta\mu$, on a time scale of ≈200 fs. This progressive increase comes about because excitation of retinal triggers a translocation of the positive charge from the protonated Schiff base toward the β-ionone end of retinal [predicted by quantum-chemical calculations (21)]. The observed rise time of the Trp response, on the order of 150–200 fs, therefore reflects the relevant time scale for the photo-induced translocation of charge preceding isomerization. Afterward, the dipole moment decreases with the time constants typical of the isomerization of retinal and vibrational relaxation of the 13-*cis* photoproduct (14). The factor of ≈1.8 increase in the amplitude of A_1 for the mutant was also reproduced by the model of excitonic coupling. It results from the three-body interactions, including nonadditive contributions, which is the case with interactions involving polarizability.

The Retinal Response. The instantaneous rise (within the cross correlation) of the F_3 component clearly speaks for a retinal signal, in sharp contrast with the slower rise of the Trp response (F_1 component). In addition, the decay times are very close to those reported in experiments probing retinal itself, either by stimulated emission (10, 31) or excited-state absorption at 460 nm (23).

Regarding the F_2 component, the steep Gaussian rise of ≈150 fs is followed by an additional rise time of ≈500 fs corresponding to the isomerization time of retinal (14) and the growth of the J intermediate, whereas the 3- to 4-ps decay and the observation of a nondecaying signal at long times resemble very much the absorption changes in the 590- to 610-nm region, caused by vibrational relaxation, and the μs lifetime of the K intermediate, respectively (3, 4, 9). Therefore, F_2 can unambiguously be identified as a near-UV signature of the photoproduct. The delayed onset of ≈250 fs and its steep rise clearly point to an impulsive formation of the photoproduct, most likely after wave packet evolution on a potential surface that is spectroscopically "dark" for the UV probe photons before ≈250 fs. As emphasized above, the delay in the appearance of the signal is not a product of the recursive kinetic data decomposition method. F_2 is detectable at 292–306 nm, where the near-UV signal is composed of not more than two components. In contrast, in VIS-pump-probe experiments the early part of the transients at 620–700 nm, commonly attributed to the J and K intermediates (3, 4, 11), is congested because of the overlapping contributions of stimulated emission and excited-state absorption (9), which do not allow isolating a specific spectroscopic signature of the photoproduct. Because the Franck-Condon windows for the probe pulse are strongly sensitive to the conformation of the molecule in polyatomic molecules, and in conjugate chains in particular (32), it is likely that the F_2 signal appears once retinal has undergone a structural change significant enough to open a new spectroscopic window for the probe pulse. This picture provides a clear confirmation to the conjectures of refs. 11, 18, and 16, which underscore this time scale as characteristic for the formation of a transient twisted excited state before isomerization.

Our pump pulses can excite high-frequency skeletal modes in 1,150–1,250 cm^{-1} (26- to 28-fs period), caused by in-plane bending coupling with the C-C stretching modes, and in 900–1,000 cm^{-1} (33- to 37-fs period) caused by hydrogen-out-of-plane (HOOP) modes (11), eventually with formation of a wave packet of the latter. These high-frequency modes will then relax to lower-frequency modes, in particular the torsional modes at 170 cm^{-1} (196 fs). In ref. 18, the decay of the C=C, C-C, and HOOP modes was determined to be 260 ± 10 fs. The large mismatch in energy between these modes and the torsional modes would lead to an indirect impulsive excitation of the latter ones. Coherent oscillations have been observed caused by torsional modes in bR, which survive up to ≈1 ps, i.e., beyond the formation time of the isomerized photoproduct (16). The same authors observed similar oscillations (but of lower frequency) in the case of protonated Schiff bases of retinal in solution. Interestingly, these oscillations appear with a phase shift, suggesting that they are not directly excited by the pump pulse. This result supports the view that the low-frequency modes are created by impulsive excitation from the high-frequency modes.

The delayed onset of F_2 is then caused by the arrival of the wave packet of the torsional mode of 170 cm^{-1} in a transition state that represents a twisted configuration, and its <150-fs initial rise reflects an impulsive formation of the latter. In principle, vibrational recurrences should have been observed in the isomerized photoproduct, superimposed on the rise or decay of the signal, as, for example, in the case of the isomerized photoproduct of rhodopsin (22). It is not unlikely that such oscillations are present in the F_2 trace, but given the small amplitude of the signals and the subtractive treatment of the data, we could not detect them. Because the recurrences are observed in *all-trans* retinal (16), the impulsive formation of the transition state on the way to the photoproduct implies that the wave packet splits in two at the branching of potential surfaces between the two isomers. Interestingly, there appears to be a sharp break in amplitude of the coherences ≈200-fs time delay in the transient absorption data of ref. 16, which may point to a splitting of the wave packet.

The above scenario agrees with the theoretical (33) and experimental evidence (9, 11, 17, 23, 34) for the so-called two-state/two-mode model. Basically, after ultrafast (<50 fs) departure from the Franck-Condon region along high-frequency skeletal modes, the molecule undergoes low-frequency torsional motion, coherently excited by the former modes, eventually leading to the isomerization of retinal.

It is interesting to note that the appearance time of ≈250 fs for F_2 is close to the time for the translocation of charge along retinal (19). This result suggests that the latter contributes to increasing the isomerization rate in proteins, as compared with the situation in solutions (35). The extent to which this effect occurs has, we propose, to do with two effects. On the one hand, the translocated positive charge at the retinal ionone ring is likely to be stabilized by dipolar and polarizable amino acid side chains [Ser-141, Thr-142, Thr-204, Trp-138, and Trp 189 (36)]. These interactions may lead to a barrier-less energy profile as a function of the torsional angle. On the other hand, and concurrent to the latter, the depletion of positive charge on the N+ atom during the excited-state lifetime will also strengthen the H bond to water402, which as a consequence may disrupt the network of H bonds with the negatively charged residues (Asp-85, Asp-212, and Arg-212) (37), and thus relax the steric hindrances on retinal.

In summary, the following sequence of events in the dynamics of bR emerges from the present results and those of the literature: (*i*) Excitation of the high-frequency skeletal modes leads to an ultrafast departure from the Franck-Condon region (<50 fs). (*ii*) These decay to low-frequency torsional modes on a sub-250-fs time scale (11, 18), exciting a wave packet of torsional modes, while translocation of charge along the retinal chain occurs (19). (*iii*) The transition state, which corresponds to a twisted (but not isomerized) configuration of retinal (11), is impulsively generated (Fig. 5). It also represents the onset for the formation of the isomerized photoproduct and appears to be formed by splitting the wave packet of torsional modes on the excited-state potential surface. (*iv*) Because the time scales are very close for formation of the transition state and translocation of charge, we believe that the latter sets the stage for the full isomerization by affecting the environment through polarization of residues and disruption of the network of H bonds, relaxing the steric hindrances to isomerization of retinal.

Materials and Methods

The experiment is based on a fs VIS-pump/UV-probe transient absorption experiment, using two noncollinear optical parametric amplifiers (NOPAs) (38), pumped at 1 kHz by 400-nm pulses derived from the 460-μJ output of a regenerative Ti:Sapphire amplifier system. The NOPAs, after compression in fused silica prisms, deliver ≈25-fs pulses tunable between 520 and 660 nm (≈1-μJ pulse energy, 40- to 55-nm spectral width). One of them is tuned to 560 nm for excitation of the retinal in bR, while the second one is frequency-doubled in a 0.15-mm-thick β-barium borate (BBO) crystal followed by a UG11 filter (Schott, Mainz, Germany) so as to remove the fundamental. The acceptance angle of the second harmonic generation crystal caused some limitation of the spectral bandwidth of the UV probe pulses, which gives us a useful spectral resolution of ≈2 nm. The width of the VIS/UV cross correlation at the position of the sample was 80–90 fs. It was measured by difference frequency mixing in a 50-μm BBO crystal placed behind a 2-mm quartz window to mimic the flow cell front window. The pump beam excitation density was ≈350 μJ/cm^2, corresponding to 30% photolysis, which was a compromise between low excitation power and high signal-to-noise ratio. For parallel polarization of pump and probe pulses, a $\lambda/2$ retarder plate rotated the linear polarization of the pump beam.

Purified purple membrane patches of WT bR and the W182F mutant isolated from *Halobacterium salinarum* were prepared in a suspension buffered at pH 7.0. In the mutant, Trp-182 is replaced by a spectrally silent phenylalanine in our probe region. The bR sample had an OD of 5.0 per cm at 568 nm and 9.0–9.5 at 280 nm (without correction for scattering). The sample was circulated by a peristaltic pump through a small-cycle volume flow cell (39) with 200-μm path length. Refreshment of the sample before each laser shot avoided accumulation of photoproducts and bleached molecules. As the sample was degraded by the UV probe light, it was exchanged on a daily basis.

The photo-induced absorption changes were monitored with a silicon photodiode in a pump/unpumped single-shot detection scheme. The probe light intensity was also measured and taken for reference. To account for scattering particles, 0.1–1% of the shots with smallest transmission were disregarded. The five subsequent time scans were averaged, i.e., each point was an average of 10,000 laser shots. The detection limit of the experiment was $\Delta OD = 10^{-4}$ to 10^{-5}, depending on the scattering behavior of the sample.

We thank J. Bredenbeck (University of Zurich, Zurich) for providing the small-volume flow cells and P. Hamm, J. Wachtveitl, G. Stock, I. H. M. van Stokkum, and G. van der Zwan for insightful discussions and valuable suggestions. Financial support was provided by Swiss National Science Foundation Grants 21-59265.99, 21-065135.01, and 2000-67912.02 and a PROFIL-2 grant (to S.H.).

1. Kochendoerfer, G. G. & Mathies, R. A. (1995) *Isr. J. Chem.* **35,** 211–226.
2. Sharkov, A. V., Pakulev, A. V., Chekalin, S. V. & Matveetz, Y. A. (1985) *Biochim. Biophys. Acta* **808,** 94–101.
3. Dobler, J., Zinth, W., Kaiser, W. & Oesterhelt, D. (1988) *Chem. Phys. Lett.* **144,** 215–220.
4. Mathies, R. A., Brito Cruz, C. H., Pollard, W. T. & Shank, C. V. (1988) *Science* **240,** 777–779.
5. Schoenlein, R. W., Peteanu, L. A., Mathies, R. A. & Shank, C. V. (1991) *Science* **254,** 412–415.
6. Du, M. & Fleming, G. R. (1993) *Biophys. Chem.* **48,** 101–111.
7. Logunov, S. L., ElSayed, M. A., Song, L. & Lanyi, J. K. (1996) *J. Phys. Chem.* **100,** 2391–2398.
8. Haran, G., Morlino, E. A., Matthes, J., Callender, R. H. & Hochstrasser, R. M. (1999) *J. Phys. Chem. A* **103,** 2202–2207.
9. Gai, F., Hasson, K. C., McDonald, J. C. & Anfinrud, P. A. (1998) *Science* **279,** 1886–1891.
10. Ye, T., Friedman, N., Gat, Y., Atkinson, G. H., Sheves, M., Ottolenghi, M. & Ruhman, S. (1999) *J. Phys. Chem. B.* **103,** 5122–5130.
11. Kobayashi, T., Saito, T. & Ohtani, H. (2001) *Nature* **414,** 531–534.
12. Haacke, S., Schenkl, S., Vinzani, S. & Chergui, M. (2002) *Biopolymers* **67,** 306–309.
13. Ruhman, S., Hou, B. X., Friedman, N., Ottolenghi, M. & Sheves, M. (2002) *J. Am. Chem. Soc.* **124,** 8854–8858.
14. Herbst, J., Heyne, K. & Diller, R. (2002) *Science* **297,** 822–825.
15. Schmidt, B., Sobotta, C., Heinz, B., Laimgruber, S., Braun, M. & Gilch, P. (2005) *Biochim. Biophys. Acta* **1706,** 165–173.
16. Hou, B., Friedman, N., Ottolenghi, M., Sheves, M. & Ruhman, S. (2003) *Chem. Phys. Lett.* **381,** 549–555.
17. Zhong, Q., Ruhman, S., Ottolenghi, M., Sheves, M., Friedman, N., Atkinson, G. H. & Delaney, J. (1996) *J. Am. Chem. Soc.* **118,** 12828–12829.
18. McCamant, D. W., Kukura, P. & Mathies, R. A. (2005) *J. Phys. Chem. B* **109,** 10449–10457.
19. Schenkl, S., van Mourik, F., van der Zwan, G., Haacke, S. & Chergui, M. (2005) *Science* **309,** 917–920.
20. Salem, L. & Bruckmann, P. (1975) *Nature* **258,** 526–528.
21. González-Luque, R., Garavelli, M., Bernardi, F., Merchán, M., Robb, M. A. & Olivucci, M. (2000) *Proc. Natl. Acad. Sci. USA* **97,** 9379–9384.
22. Wang, Q., Schoenlein, R. W., Peteanu, L. A., Mathies, R. A. & Shank, C. V. (1994) *Science* **266,** 422–424.
23. Hasson, K. C., Gai, F. & Anfinrud, P. A. (1996) *Proc. Natl. Acad. Sci. USA* **93,** 15124–15129.
24. Beechem, J. M., Amelot, M. & Brand, L. (1985) *Chem. Phys. Lett.* **120,** 466–472.
25. Knutson, J. R., Beechem, J. M. & Brand, L. (1983) *Chem. Phys. Lett.* **102,** 501–507.
26. Satzger, H. & Zinth, W. (2003) *Chem. Phys.* **295,** 287–295.
27. Croce, R., Muller, M. G., Bassi, R. & Holzwarth, A. R. (2001) *Biophys. J.* **80,** 901–915.

28. Holzwarth, A. (1996) in *Biophysical Techniques in Photosynthesis*, eds. Amesz, J. & Hoff, J. A. (Kluwer, Amsterdam), pp. 75–92.
29. Huang, J., Chen, Z. & Lewis, A. (1989) *J. Phys. Chem.* **93,** 3314–3320.
30. Mathies, R. A. & Stryer, L. (1976) *Proc. Natl. Acad. Sci. USA* **73,** 2169–2178.
31. Kennis, J. T. M., Larsen, D. S., Ohta, K., T, F. M., Glaeser, R. M. & Fleming, G. R. (2002) *J. Phys. Chem. B* **106,** 6067–6080.
32. Blanchet, V., Zgierski, M. Z., Seidemann, T. & Stolow, A. (1999) *Nature* **401,** 52–54.
33. Garavelli, M., Negri, F. & Olivucci, M. (1999) *J. Am. Chem. Soc.* **121,** 1023–1029.
34. Haran, G., Wynne, K., Xie, A., He, Q., Chance, M. & Hochstrasser, R. M. (1996) *Chem. Phys. Lett.* **261,** 389–395.
35. Zgrablic, G., Voitchovsky, K., Kindermann, M., Haacke, S. & Chergui, M. (2005) *Biophys. J.* **88,** 2779–2788.
36. Aharoni, A., Khatchatouriants, A., Manevitch, A., Lewis, A. & Sheves, M. (2003) *J. Phys. Chem. B* **107,** 6221–6225.
37. Luecke, H., Schobert, B., Richter, H.-T., Cartailler, J.-P. & Lanyi, J. K. (1999) *J. Mol. Biol.* **291,** 899–911.
38. Riedle, E., Beutter, M., Lochbrunner, S., Piel, J., Schenkl, S., Spörlein, S. & Zinth, W. (2000) *Appl. Phys. B* **71,** 457–465.
39. Bredenbeck, J. & Hamm, P. (2003) *Rev. Sci. Instrum.* **6,** 3188–3189.
40. Eftink, M. R., Selvige, L. A., Callis, P. R. & Rehms, A. A. (1990) *J. Phys. Chem.* **94,** 3469–3479.